

## Initial experiments with a versatile multi-aperture negative-ion source and related improvements

M. CAVENAGO(\*)

*INFN, Laboratori Nazionali di Legnaro - v.le dell'Università 2, I-35020 Legnaro, Italy*

received 5 February 2016

**Summary.** — A relatively compact ion source, named NIO1 (Negative-Ion Optimization 1), with 9 beam apertures for  $H^-$  extraction is under commissioning, in collaboration between Consorzio RFX and INFN, to provide a test bench for source optimizations, for innovations, and for simulation code validations in support of Neutral Beam Injectors (NBI) optimization. NIO1 installation includes a 60 kV high-voltage deck, power supplies for a 130 mA ion nominal current, an X-ray shield, and beam diagnostics. Plasma is heated with a tunable 2 MHz radiofrequency (rf) generator. Physical aspects of source operation and rf-plasma coupling are discussed. NIO1 tuning procedures and plasma experiments both with air and with hydrogen as filling gas are described, up to a 1.7 kW rf power. Transitions to inductively coupled plasma are reported in the case of air (for a rf power of about 0.5 kW and a gas pressure below 2 Pa), discussing their robust signature in optical emission, and briefly summarized for hydrogen, where more than 1 kW rf power is needed.

### 1. – Introduction

Sources of negative ions of hydrogen isotopes [1, 2] are used in nuclear fusion and acceleration technology, so that a detailed understanding of ion production and extraction from plasma is both challenging for designers and important for these applications [3-5]. This paper describes a negative-ion source (built and operated in collaboration between Consorzio RFX and INFN, see later and in sect. 2), which is compact enough to make modifications, training, test of new ideas and validations of simulation models possible, aiming to provide a reduced-size model of the giant negative-ion sources and accelerators under construction for nuclear-fusion researches.

Magnetically confined nuclear-fusion reactors, as the International Thermonuclear Experimental Reactor (ITER) under construction and the DEMONstration Power Plant

---

(\*) E-mail: [cavenago@lnl.infn.it](mailto:cavenago@lnl.infn.it)

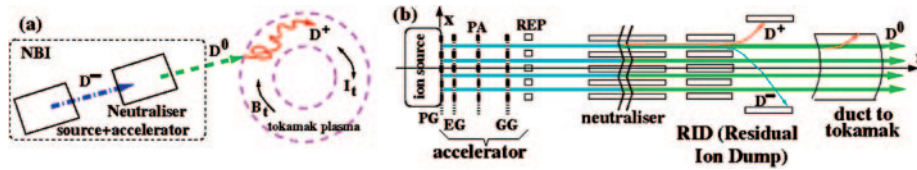


Fig. 1. – a) NBI heating for tokamaks; b) scheme of a NBI unit and parts; the accelerator electrode names and numbers may vary (PA, GG or repeller REP may be also omitted).

(DEMO) under design [3], envision additional heating of plasma by several methods, including the neutral beam injectors (NBI) [4,6], see fig. 1; typically (as in the NBI units for ITER), a beam of  $D^-$  is accelerated to 1 MeV (total beam current 40 A divided in 1280 beamlets) and then partly converted with a gas neutralizer to  $D^0$ , which are not deviated by tokamak magnetic field  $\mathbf{B}$  (with toroidal  $B_t$  and poloidal  $B_p$  field components).

Challenges in developing suitable negative-ion sources are related to the following physical reasons. The electron affinity of H isotopes is small enough (0.76 eV) to have a large cross section for  $H^-$  neutralization (larger than  $H^+$  one at stated beam energy [4]); on the other side, producing and maintaining  $H^-$  requires a plasma electron temperature  $T_e$  in the eV order. Ion source is therefore divided in to two zones: the driver plasma (heated with radiofrequency) where  $T_e \geq 4$  eV, as requested for  $H_2$  (or  $D_2$ ) ionization balance, and the extraction plasma where electron temperature is reduced by a magnetic filter (see fig. 2(a)) and  $H^-$  may be produced (by collisions of H and  $H^+$  against cesiated wall or by  $e^-$  attachment to vibrationally excited  $H_2$  molecules). Due to the large total area  $A_e$  (subdivided in many apertures) of beam extraction, the gas pressure  $p_1$  inside the source must be limited,  $p_1 < 1$  Pa, to maintain accelerator pressure  $p_2$  low enough ( $< 0.1$  Pa) to avoid electrode discharge and to make vacuum system affordable. The pressure inside the source must be high enough to maintain plasma and to have enough production of  $H^-$ . The assumed reference value for ITER sources is  $p_1 = 0.3$  Pa, with a  $240 \text{ A/m}^2$   $D^-$  extracted current density, mostly produced thanks to an adequate Cs wall coverage; a reduction or elimination of Cs usage is a goal of DEMO development.

Major issues for source design are therefore the radiofrequency coupling as a function of the pressure and the source geometry,  $H^-$  production and wall chemistry, the optimal magnet configuration, and the extraction electrode shapes. The reduced size and the modular design of NIO1 (Negative Ion Optimization 1) are planned to make systematic investigation of these issues possible.

NIO1 is a radiofrequency (rf) ion source as the larger sources [7], like SPIDER [8] (Source for Production of Ion of Deuterium Extracted from RF plasma) under construction for the neutral beam injectors [9,10]. The rf power is applied to a coil wound over a dielectric tube (called rf window) which is a part of the plasma chamber, see fig. 2; other parts of the plasma chamber (sealed with Viton O-rings) are made of copper, with adequate cooling; the water-cooled rf coil is encased into a plastic cover. Permanent magnets (PM) for plasma confinement are encased into this plastic cover and into copper walls.

A so-called Faraday shield (a slotted copper structure protecting the rf window from plasma impact) was not installed in NIO1 first experiments, to study a more efficient rf coupling in a new and simpler geometry. Some cooling of rf window is provided by compressed air, flowing into channels milled into the rf coil plastic cover; moreover the thermal expansion of the rf window is mechanically allowed.

Simpler plasma models assume the coil voltage is shielded (by a plasma surface layer or by a Faraday shield), so that only induction field penetrates the plasma [11,12]; this is the

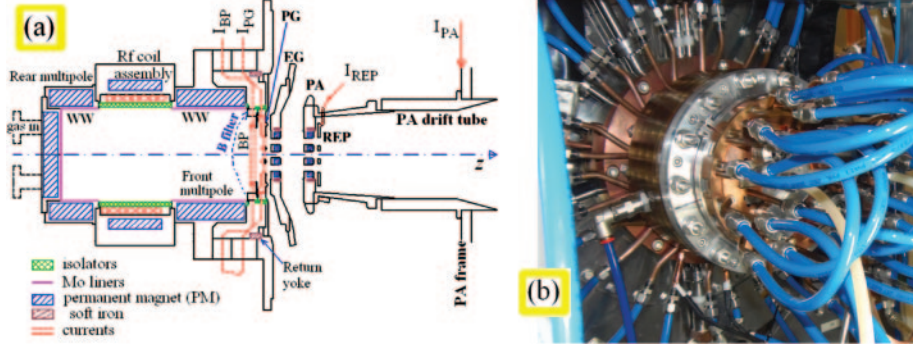


Fig. 2. – a) Section of NIO1 source and acceleration electrodes EG, PA and REP; b) view of NIO1 source, air input to coil assembly in foreground; rear multipole is partly covered by water cooling connection.

inductively coupled plasma (ICP or so-called H-mode). At low electron density  $n_e$  with insufficient shielding, the large coil voltage may accelerate plasma electrons (E-mode) and disturb plasma confinement [13]; these E- and H-modes should not be confused with the low- and high-confinement modes (L- and H-modes) of a tokamak [3]. Even if a complete theory is missing, the transition from E- to H-mode results in a sharp increase of plasma light emission, for a small rf power increase, especially at low gas pressure, as confirmed experimentally [14, 15]; effects on electron temperature are later discussed. Distinction between these modes (described in simpler geometries of rf planar coil [16]) is thus of primary importance for ion source modelling and efficiency [17].

The rest of the paper is organized as follows. Some remarks on DEMO efficiency are detailed next. In sect. 2, the recent improvements to NIO1 setup are summarized. Plasma coupling models are briefly discussed in sect. 3; also the rapidly growing 3D numerical models on NIO1 are referenced. Experimental results with air and hydrogen are discussed in sect. 4.

**1.1. Notes on DEMO efficiency quest.** – In ITER (and probably DEMO) specifications [3, 4], additional heating methods (with total power  $P_d$  delivered to plasma) are needed because: 1) on the torus axis,  $B_t \cong 5.3$  T for practical limits of reliable superconductive cables, so that plasma density is limited  $n_e \cong 10^{20} \text{ m}^{-3}$  and the fusion reaction is not self-supporting (the so-called ignition regime), even if the total produced thermal power  $P_p$  is larger than  $P_d$  (break even regime). Let  $Q = P_p/P_d$ ; in the ITER design,  $P_p = 0.5$  GW and expected  $Q$  ranges from 5 to 10; 2) a toroidal current  $I_t$  circulating into plasma is needed for stability; NBI (and some other heating methods) must have the so-called “current drive” capability, that is, they should give a contribution to  $I_t$ , in addition to transient effects of tokamak fields.

In the perspective of electric power  $P_e$  production of DEMO, both  $Q$  and the efficiency  $\eta_d$  of heating methods (defined as the ratio of average  $P_d$  to average plug power  $P_a$ ) must be improved, to at least  $\eta_d > 0.4$ ; note that conversion rate  $\eta_e = P_e/P_p$  (from thermal to electric power  $P_e$ ) is also limited, optimistically  $\eta_e \cong 0.45$ . The global efficiency criterion

$$(1) \quad \eta_g \equiv \eta_e Q \eta_d > 1$$

must be satisfied for operation (and  $\eta_g \gg 1$  for effective economic operation). In comparison to other heating methods, NBI offer advantages for current drive (depending on beam aiming and energy) and present some difficulties as concerns efficiency  $\eta_d$ , depending on the large number of components in NBI; which makes source optimization even more necessary.

## 2. – NIO1 setup overview

Some schemes and views of the NIO1 source are given in figs. 2 and 3, while design is reviewed elsewhere [17-19]. Both operation with air and with hydrogen were performed, while operation with deuterium is of course excluded (for easy maintenance and improvements); nitrogen or oxygen tests are also planned. The plasma chamber is approximately a 0.21 m long cylinder with inner radius  $r_w = 0.05$  m; the rf window was made of alumina and now is made of a borosilicate glass (Pyrex), as used in a test stand, named MetAlice, where a small rf plasma generator was installed to help NIO1 design [20]. One cylinder base, named the plasma grid PG, has 3 rows of 3 holes for beam extraction (hole diameter 7.6 mm, spacing 14 mm) for a 130 mA maximum total ion current; before PG, a collimator named bias plate BP with a  $52 \times 58$  mm opening is placed inside the plasma, to help the action of the magnetic filter. Both BP and PG are insulated from the other metallic walls (WW) of the plasma chamber, so that a bias voltage  $V_b = V_{PG} - V_{WW} \cong 10$  V can be applied [2,7], and currents ( $I_{PG}$  and  $I_{BP}$  up to 400 A) for additional magnetic filtering can be circulated. Source is made of six easily separable modules (sealed with elastomer O-rings), namely the rear cover, the rear multipole, the rf coil assembly, the front multipole, the BP assembly and the PG assembly. Each assembly has electrical and/or water connections as necessary; some modules have CF16 ports for optical observation, cesium and gas input, or pressure measure. Also the acceleration column is composed of high voltage (HV) alumina insulators and modules, mainly the column base, the Extraction Grid (EG) assembly and the post accelerator (PA) electrode assembly. In nominal design, PG is held to  $-60$  kV and EG to  $-52$  kV, while PA is connected to a ground potential via a shunt resistor (clamped to  $\pm 35$  V); the beam current  $I_{PA}$  flowing into PA can be inferred by a voltmeter readout (so that interferences from rf are negligible). For initial commissioning, PG voltage is limited to  $-20$  kV (with EG voltage limited within 5 kV with respect to PG).

Acceleration column and source with horizontal beam axis  $z$  are cantilevered on the column base, bolted to the rest of the vacuum vessel (a 1.8 m long, 0.35 m inner diameter

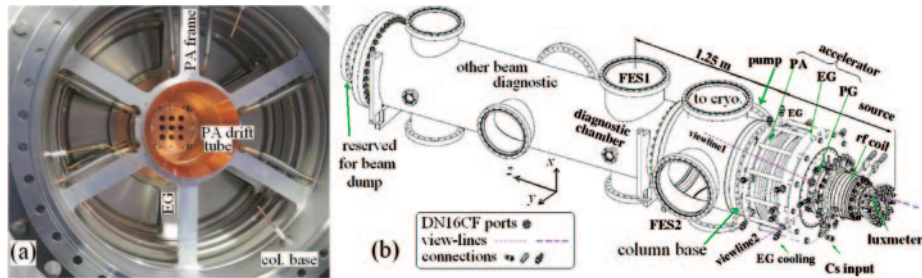


Fig. 3. – a) View looking inside the accelerating column, with its base and the PA in the foreground; note the nine holes for beam passage; b) isometric view of NIO1.

tube where several diagnostic and pump ports are provided). Source is enclosed in a HV deck (HVD) where the rf generator, its matching box, the BP and PG power supplies, dosing gas valves and some control electronics are located. All area is enclosed by a soft X-ray shield, with usual safety procedures [18]. The 2 MHz rf generator is connected to the rf coil by a simple matching box [13], with two capacitors  $C_a$  and  $C_b$ , see fig. 4(b); let  $R_1$  and  $L_1$  be respectively the resistance and the inductance seen at coil ends (possibly including plasma reaction). During NIO1 operation, forward rf power  $P_f$  can be set from 0.05 to 2.5 kW, while frequency  $f$  can be adjusted (by  $\pm 10\%$ ); the generator provides an approximate digital reading of  $P_f$  and reflected rf power  $P_r$ . These parameters ( $P_f$ ,  $P_r$ ,  $f$ ,  $C_a$  and  $C_b$ ) can give information on energy transfer between rf coil and plasma electrons (which depends both on  $e^-$ -gas collisions and on stochastic heating [13, 16]), to compare with plasma model (provided that rf connections and transmission lines are adequate). Note that  $C_a$  and  $C_b$  can be now regulated with power off only, both on NIO1 and on MetAlice. By trial and error adjustments, coil resonance on MetAlice was progressively optimized, ending with  $C_a = 3.08$  nF,  $C_b = 16.3$  nF and  $f = 1.96$  MHz: final results for small signal tests are shown in fig. 4(c); note the very good agreement with the model (due to the use of coaxial lines) and the input impedance at resonance  $Z_0 = 130$  ohm, due to a small load  $R_1 = 0.177$  ohm, which gives a large reflection factor  $R_{\text{eff}} = P_r/P_f \cong 0.17$ . When rf power is applied, the plasma load reduces the LCR quality factor, so that  $Z_0$  reduces, approaching the no reflection condition ( $Z_0 = 50$  ohm) for  $P_f = 250$  W; then  $P_r \leq 3$  W (resolution limit), as desired. A matching of NIO1 was similarly performed (ending with  $C_a = 2.13$  nF,  $C_b = 9.14$  nF and  $f = 2.01$  MHz); without plasma  $Z_0 \cong 80$  ohm and  $R_1 \cong 0.8$  ohm; with plasma, reflection depends on the regime investigated, with  $P_r/P_f$  typically ranging from 0.01 to 0.2.

For budget reasons, only one recovered turbopump is now installed: pumping speed  $S$  is adequate for air experiments ( $S \cong 0.5$  m<sup>3</sup>/s), but it decreases to  $S = 0.1$  m<sup>3</sup>/s for

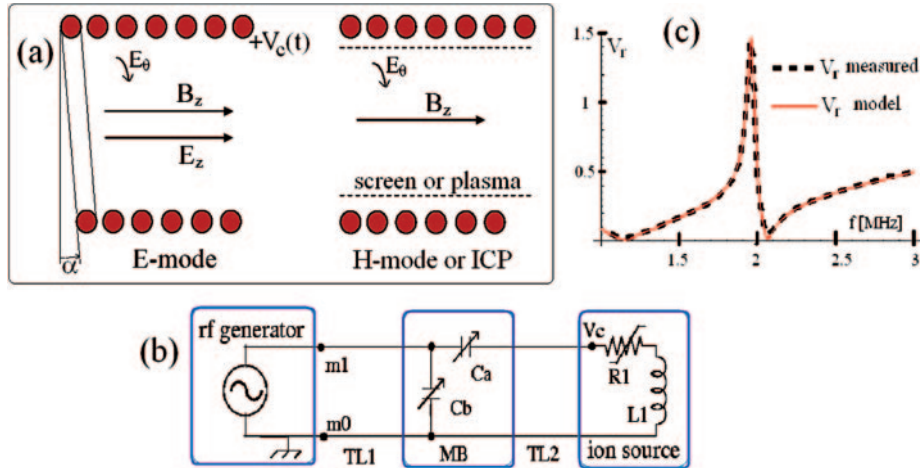


Fig. 4. – a) Coil sections, with field patterns in E-mode and H-mode; b) simplified equivalent scheme of rf coil; the matching box MB is connected by transmission lines, TL1 and TL2, to generator and to source coil, with effective resistance  $R_1$  strongly dependent from plasma density; m0 and m1 are the points used in the  $Z_0$  impedance measurement; c) voltage ratio  $V_r$  with no plasma.

a typical maximum hydrogen flow of  $0.1 \text{ Pa m}^3/\text{s}$ . Since source-to-vessel conductance is  $C_1 = 0.1 \text{ m}^3/\text{s}$  [21], typical pressures are  $p_2 = 1 \text{ Pa}$  and  $p_1 = 2 \text{ Pa}$  for hydrogen, which somewhat limits source and accelerator experimental range. Installation of two additional cryogenic pumps is planned for 2016. Improvement of cooling-water resistivity is also pursued (by installation of suitable filters and pipe materials).

A high-resolution (0.05 nm) spectrometer, for atomic and molecular detailed optical diagnostic [22], is installed on NIO1. Also a low- (1 nm) resolution spectrometer is installed in NIO1, which can collect data on the [300, 850] nm range all at once, in an integration time  $t_i$ ; this instrument is thus used for real-time plasma monitoring (detection of impurities) and spectra recording: let  $M_{394}$  be the intensity of the  $\lambda = 394.3 \text{ nm}$  line [23, 24], a radiative line from  $\text{N}_2$ , excited by electrons with kinetic energy  $K_e \geq 11 \text{ eV}$  (with maximum cross section at 16 eV);  $M_{391}$  be the intensity of the  $\lambda = 391.4 \text{ nm}$  line from radiative decay of  $\text{N}_2^+$ , excited by impact of electrons with kinetic energy  $K_e \geq 18 \text{ eV}$  (with maximum cross section at 100 eV) [25]. For comparison with  $M_{394}$  we have two luminosity measurement:  $L_x$  from a luxmeter (placed onto a CF16 port on NIO1 rear cover) and  $P_{\text{pmt}}$  the incident power onto a calibrated photomultiplier (PMT) detector, connected to NIO1 with a fiber optic and an imaging system. Most important, in a pure nitrogen plasma the ratio  $M_{391}/M_{394}$  results in a given increasing function  $f$  of  $T_e$ , provided deviations from a Maxwellian distribution are neglected [23]; let us define the inferred temperature  $T_e = f^{-1}(M_{391}/M_{394})$ , which can be easily computed for any nitrogen mixture.

### 3. – Overview of models and simulations of NIO1

Let us consider first the case  $n_e \rightarrow 0$  (as relevant to E-mode or to preglow condition, with no Faraday shield) [12]. Let  $\ell, r_c, N$  be respectively the coil length, average radius and number of turns, while the current flowing in the coil is written  $\Re I_c e^{i\omega t}$ , or more frequently  $I_c$ , leaving the harmonic factor understood (phasor notation). For simplicity of the following discussion, long solenoid ( $\ell \gg r_c$ ) and quasistatic ( $\omega r_c/c \ll 1$ ) approximations are used. Then  $B_z \cong \mu_0 I_c N/\ell$  inside the coil, and  $E_\vartheta = -i\omega r B_z/2$  for  $r \leq r_c$ . The axial electric field is  $E_z \cong V_c/\ell$  with  $V_c$  the voltage applied to the coil. In the case  $R_1 \ll \omega L_1$  (coil resistance negligible) we have  $V_c = i\omega L_1 I_c$  from simple circuit theory, and then  $E_z = i\pi\omega\mu_0 I_c (r_c N/\ell)^2$ ; note the simple ratio of  $E_\vartheta(r_c)$  at coil  $r = r_c$  and  $E_z$

$$(2) \quad \frac{|E_\vartheta(r_c)|}{|E_z|} = \frac{\ell}{2\pi r_c N} = \tan \alpha,$$

where  $\alpha \ll 1$  is the pitch angle used to wind coil; this (perhaps unexpected) ratio is confirmed by field calculations [26] and measurements [27]. In this field pattern, for some rf phase, electrons can be accelerated up to energies of the order of  $|eV_c|$ , when  $I_c \geq I_0 = m\omega\ell^2/2eL_1$ .

At high gas densities  $n_g$ , electron-neutral collision frequency  $\nu_m = k_1 n_g$  is larger than  $\omega$  (and relevant cyclotron frequency  $\Omega_c$ ), so that plasma conductivity  $\sigma$  is a scalar number ( $\mathbf{E} = \mathbf{j}/\sigma$  with  $\mathbf{j}$  current density), given by a local Drude model

$$(3) \quad \sigma = \frac{e^2}{m} \frac{n_e}{\nu_m + i\omega}.$$

Ponderomotive force  $F_m$  and heating power density  $P_h$  are then

$$(4) \quad F_m = -\frac{e^2}{4m} \frac{\nabla|\mathbf{E}|^2}{(\nu_m)^2 + \omega^2}, \quad P_h = \frac{1}{2} \Re(\sigma \mathbf{E}) \cdot \mathbf{E} = \frac{e^2}{2m} \frac{\nu_m n_e |\mathbf{E}|^2}{(\nu_m)^2 + \omega^2},$$

where the  $\frac{1}{2}$  factor comes from time averaging. When  $n_g < \omega/k_1$  non-local effects become important, that is: electrons may be reflected by the sheath potential near walls (a wall collision); electrons may be deflected by rf and static magnetic field [12], and rf electric field (depending on  $r$ ) varies while electrons move through plasma. Most of these effects are roughly modelled as additional collisions, so that eq. (3) is still used, with an effective collision rate  $\nu_{\text{eff}}$  [28, 29] (of course, at large  $n_e$  also Coulomb collisions contribute).

Thus at small  $n_e$ , a  $j_z$  current component is driven; this current makes a  $B_\theta$  contribution and it accumulates oscillating charges near coil end (shielding  $E_z$ ), in proportion to  $n_e$ .

Even if a complete theory of E- and H-mode is still missing, some important physical trends can be noted: the power  $P_h$  delivered to plasma is proportional to  $n_e$ , which is produced by ionization, increasing with  $P_h$  and confinement; so that a sharp transition of density should be expected. Moreover, even if transition between E- and H-modes is more frequently described with planar coil [16], the cylindrical geometry favours H-mode discharges, since ponderomotive forces help plasma confinement, while in planar geometry they push plasma far away from the coil. Results of simple ICP models [11, 29, 12] show a large spread of predicted  $T_e$  (from 3 to over 10 eV), depending on transport model and absorbed power  $P_h$ , and decreasing with gas pressure; in most cases, plasma density  $n_e$  increases rapidly over a given threshold  $I_1$  for the coil current  $I_c$ , ranging from  $I_1 \cong 15$  A for air [29] at  $p_1 = 1$  Pa to larger values for hydrogen  $I_1 \cong 35$  A [12].

Due to reduced size of NIO1, several other calculations were possible in 3D (three dimensional) geometry. The gas flow in NIO1 was calculated [21], both with constant gas temperature  $T_g = 300$  K (plasma off), and with a prescribed gas heating  $T_g = 1000$  K in a plasma chamber followed by cooling because of molecule-wall collision. In the former case results confirm the  $p_1/p_2$  ratio for air (about 20) and hydrogen (about 2), and the latter case was similar.

In 3D PIC (Particle In Cell) simulations of extraction [30], the  $\text{H}^-$  beam has a denser central core, which needs further consideration in following beam transport. The production of secondary beams (due to collisions with gas inside the acceleration column) was also calculated, improving the existing 3D codes [31]. Results confirm a good transmission of  $\text{H}^-$  beam, and also important, almost a complete stop of co-extracted electron on the EG, so corroborating the column design. Equipment for beam energy recovery in ranges of voltage and current suitable for experiments with NIO1 was also modelled [32].

#### 4. – Experimental results

In NIO1 (similarly to MetAlice test stand) plasma is typically started at a large pressure  $p_1 \cong 10$  Pa and low rf power  $P_f \geq 0.05$  W; at this power, a large integration time  $t_i \cong 5$  s is required to detect spectra; the plasma onset is confirmed by  $P_{\text{pmt}}$  and  $M_{394}$  signals [19]. Rising  $P_f \geq 0.3$  kW allows to progressively reduce  $t_i \rightarrow 0.2$  s, with luminosity increase confirmed by  $P_{\text{pmt}}$ ,  $M_{394}$  and  $L_x$ , see fig. 5(a) and (b); this simplifies data acquisition. So experiments concentrated on  $P_f$  from 0.3 kW to 0.85 kW and  $p_1$  ranging from 0.36 Pa to 11.6 Pa.

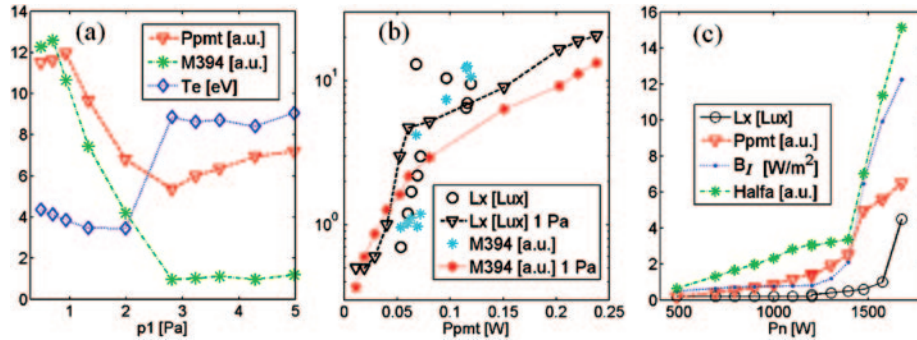


Fig. 5. – a) Plasma luminosity  $P_{\text{pmt}}$  vs. source pressure  $p_1$  (air) at constant net rf power  $P_n = P_f - P_r = 0.47$  kW;  $M_{394}$  (1 a.u. =  $10^{17}$  ph/s/m<sup>2</sup>) and  $T_e$  (typical error  $\pm 10\%$ ) are also shown; b) luxmeter readout  $L_x$  and  $M_{394}$  vs.  $P_{\text{pmt}}$ , at constant pressure ( $p_1 = 1$  Pa, lines with markers) or rf power ( $P_n = 0.47$  kW, isolated markers); c) Balmer line  $H_{\alpha}$  (1 a.u. =  $10^{17}$  ph/s/m<sup>2</sup>) and irradiance  $B_I$  vs. net rf power  $P_n$ , at constant  $H_2$  pressure  $p_1 = 2$  Pa;  $L_x$  and  $P_{\text{pmt}}$  (1 a.u. = 10 mW) are also shown.

By reducing pressure  $p_1$  at fixed rf power, a transition to a brighter plasma is obtained, see fig. 5(a); identification of this latter regime with H-mode is reasonable [17]. The same transition may be obtained by increasing power  $P_f$  over a threshold  $P_t$  at constant  $p_1$  pressure [17]; for example  $P_t = 0.5$  kW at  $p_1 \cong 1$  Pa and with good wall condition. The correlation of  $P_{\text{pmt}}$ ,  $L_x$  and  $M_{394}$  rising  $P_f$  at constant  $p_1 \cong 1$  Pa is shown in fig 5(b). The H-mode has some hysteresis, that is we need to decrease  $P_f$  by some amount (about 20%) below  $P_t$  to go back to E-mode; larger hystereses (about 50% in coil current  $I_c$ ) were observed for argon [14]. The data for fig. 5(a) were assembled from several scans rising  $P_f$  at different  $p_1$ , so to avoid ambiguity due to hystereses; this procedure also allows to compare data with net power constant  $P_n = P_f - P_r$ . Inferred temperature  $T_e$  results in 4 eV for the H-mode, in agreement with global ionization models [13]; the significance of  $T_e \cong 9$  eV for the E-mode region is that electron distribution is not maxwellian, containing a tail of energetic electrons over 20 or 30 eV, easily due to acceleration from  $V_c$  voltage. For example, with  $L_1 = 3.5 \mu\text{H}$  (NIO1 coil last measurement),  $|V_c/I_c| = 44$  ohm, that is  $V_c$  is in the kV order.

**4.1. Experiments with  $H_2$ .** – In general, hydrogen plasmas require more rf power to turn on and they produce less light. This was expected since static discharges in hydrogen require more voltage to start than in air or nitrogen, at low pressure  $p_1 \ell < 1$  Pa m [33]. So a larger range of power  $P_r$  was needed, from 0.1 up to 1. kW; only the pressure range from 0.1 to 3 Pa was partly investigated (also because alumina rf window had a failure, possibly due to unbalanced compression of mounting bolts and thermal stresses). Some plasma macroscopic features are shown in fig. 5(c), while the much more difficult spectra analysis is discussed elsewhere [22];  $B_I$  is a calculated irradiance. First, luxmeter readout was rarely over the noise level ( $L_x > 0.5$  Lux) until  $P_f > 1.3$  kW, while photomultiplier detector gain was increased to appreciate smaller  $P_{\text{pmt}}$ . To obtain a transition similar to E-H transition in air, a power rise from 1.4 to 1.7 kW at  $p_1 = 2$  Pa was needed; so  $L_x$  rose from 0.5 to 4.5 Lux and  $P_{\text{pmt}}$  from 25 mW to 64 mW, which is consistent with an inductively coupled plasma (H-mode).

For  $P_f = 1.2 \pm 0.2$  kW, it is difficult to assume a pure E-mode (from circuit model estimate); a mixture of E- and H-modes is more probable. More experiments are needed

to clarify whether this intermediate regime and the differences with air experiment E-H transitions are due to the electrical conductivity and plasma kinetic of hydrogen, are simply due to hydrogen different emissivity, or are simply circumstantial, that is due to poor condition of the rf window.

After dismounting the alumina window for substitution, two conductive rings were noted on its inner surface; this can modify  $E_z$  and  $E_\vartheta$  field pattern. Black burnings were visible on the copper walls, resembling but not exactly matching the symmetry of magnet poles. The rf window is now temporarily replaced with a Pyrex one, the air flow over rf window was increased, while most copper walls (WW) are now covered by 0.5 mm thick Mo foils (carefully machined so they fit inside, with less than a 0.1 mm tolerance) in order to reduce wall sputtering. After this maintenance and minor decrease of plasma volume, beam extraction tests, with H<sub>2</sub> or air as filling gases, have begun recently.

*4.2. Conclusions and perspectives.* – The experiments with air have confirmed the distinction between E- and H-modes, also thanks to the clear change of the inferred electron temperature, observable from nitrogen lines, consistently with the discussed physical features of these modes. Experiments with pure oxygen or pure nitrogen are planned to better study, respectively, beam extraction or spectra. Experiments with pure hydrogen have requested additional adjustments; identification of E-to-H transition is mostly based on gross luminosity jump, so that mixing H<sub>2</sub> with tracer gases (Ne, Kr [15]) may be considered. Beam extraction optimization is also in progress.

\* \* \*

I thank many colleagues and collaborators for contributing to the work and researches described in this paper, including: G. Serianni, M. Barbisan, M. De Muri, P. Agostinetti, V. Antoni, C. Baltador, L. Baseggio, M. Bigi, M. Cazzador, V. Cervaro, F. Degli Agostini, E. Fagotti, N. Ippolito, T. Kulevoy, B. Laterza, M. Maniero, A. Mimo, A. Minarello, R. Pasqualotto, S. Petrenko, D. Ravarotto, M. Recchia, E. Sartori, M. Sattin, F. Taccogna, V. Variale, B. Zaniol and P. Veltri. Work set up in collaboration and financial support of INFN (Group 5 and E), Consorzio RFX, F4E, and EUROfusion.

## REFERENCES

- [1] DUDNIKOV V., *Rev. Sci. Instrum.*, **83** (2012) 02A708.
- [2] BACAL M., *Rev. Sci. Instrum.*, **83** (2012) 02B101.
- [3] ZOHN H., ANGIANI C., FABLE E., FEDERICI G., GANTENBEIN G., HARTMANN T., LACKNER K., POLI E., PORTE L., SAUTER O., TARDINI G., WARD D. and WISCHMEIER M., *Nucl. Fusion*, **53** (2013) 073019.
- [4] HEMSWORTH R. S. *et al.*, *Nucl. Fusion*, **43** (2003) 851.
- [5] FUBIANI G., DE ESCH H. P. L., SIMONIN A. and HEMSWORTH R. S., *Phys. Rev. ST Accel. Beams*, **11** (2008) 014202.
- [6] KOJIMA A., HANADA M., TANAKA Y., INOUE T., WATANABE K., TANIGUCHI M., KASHIWAGI M., UMEDA N., TOBARI H., GRISHAM L. R. and JT-60 NBI GROUP, *Rev. Sci. Instrum.*, **81** (2010) 02B112.
- [7] KRAUS W., FANTZ U., FRANZEN P., FRÖSCHLE M., HEINEMANN B., RIEDL R. and WÜNDERLICH D., *Rev. Sci. Instrum.*, **83** (2012) 02B104.
- [8] AGOSTINETTI P., ANTONI V., CAVENAGO M., CHITARIN G., MARCONATO N., MARCUZZI D., PILAN N., SERIANNI G., SONATO P., VELTRI P. and ZACCARIA P., *Nucl. Fusion*, **51** (2011) 063004.
- [9] TAKEIRI Y., *Rev. Sci. Instrum.*, **81** (2010) 02B114.

- [10] ZACCARIA P., AGOSTINETTI P., MARCUZZI D., PAVEI M., PILAN N., RIZZOLO A., SONATO P., SPADA F. and TREVISAN L., *Rev. Sci. Instrum.*, **83** (2012) 02B108.
- [11] TUSZEWSKI M., *Phys. Plasmas*, **5** (1998) 1198.
- [12] CAVENAGO M. and PETRENKO S., *Rev. Sci. Instrum.*, **83** (2012) 02B503.
- [13] LIEBERMAN M. A. and LICHTENBERG A. J., *Principles of Plasma Discharges and Material Processing* (John Wiley, New York) 1994.
- [14] KORTSHAGEN U., GIBSON N. D. and LAWLER J. E., *J. Phys. D: Appl. Phys.*, **29** (1996) 1224.
- [15] ABDEL-RAHMAN M., SCHULZ-VON DER GATHEN V. and GANS T., *J. Phys. D: Appl. Phys.*, **40** (2007) 1678.
- [16] LISHEV ST., SHIVAROVA A., TARNEV KH., IORDANOVA S., KOLEVA I., PAUNSKA TS. and IORDANOV D., *J. Phys. D: Appl. Phys.*, **46** (2013) 165204.
- [17] CAVENAGO M., SERIANNI G., DE MURI M., AGOSTINETTI P., ANTONI V., BALDADOR C., BARBISAN M., BASEGGIO L., BIGI M., CERVARO V., DEGLI AGOSTINI F., FAGOTTI E., KULEVOY T., IPPOLITO N., LATERZA B., MINARELLO A., MANIERO M., PASQUALOTTO R., PETRENKO S., POGGI M., RAVAROTTO D., RECCHIA M., SARTORI E., SATTIN M., SONATO P., TACCOGNA F., VARIALE V., VELTRI P., ZANIOL B., ZANOTTO L. and ZUCCHETTI S., *Rev. Sci. Instrum.*, **87** (2016) 02B320.
- [18] DE MURI M., CAVENAGO M., SERIANNI G., VELTRI P., BIGI M., PASQUALOTTO R., BARBISAN M., RECCHIA M., ZANIOL B., KULEVOY T., PETRENKO S., BASEGGIO L., CERVARO V., DEGLI AGOSTINI F., FRANCHIN L., LATERZA B., MINARELLO A., ROSSETTO F., SATTIN M. and ZUCCHETTI S., *Fusion Eng. Des.*, **96** (2015) 249.
- [19] CAVENAGO M., SERIANNI G., ANTONI V., BIGI M., DE MURI M., PASQUALOTTO R. *et al.*, *AIP Conf. Proc.*, **1655** (2015) 040006.
- [20] CAVENAGO M., KULEVOY T., PETRENKO S., ANTONI V., BIGI M., FELLIN F., RECCHIA M., SERIANNI G. and VELTRI P., *Rev. Sci. Instrum.*, **83** (2012) 02A707.
- [21] SARTORI E., VELTRI P., CAVENAGO M. and SERIANNI G., *Rev. Sci. Instrum.*, **87** (2016) 02B118.
- [22] BARBISAN M., BALDADOR C., ZANIOL B., CAVENAGO M., FANTZ U., PASQUALOTTO R., SERIANNI G., VIALETTA L. and WÜNDERLICH D., *Rev. Sci. Instrum.*, **87** (2016) 02B319.
- [23] BRITUN N., GAILLARD M., RICARD A., KIM Y. M., KIM K. S. and HAN J. G., *J. Phys. D: Appl. Phys.*, **40** (2007) 1022.
- [24] BEHRINGER K. and FANTZ U., *J. Phys. D: Appl. Phys.*, **27** (1994) 2128.
- [25] ITIKAWA Y., *J. Phys. Chem. Ref. Data*, **35** (2006) 31.
- [26] HENJES K., *J. Appl. Phys.*, **79** (1996) 21.
- [27] LEE S., LEE Y. and YU I., *Jpn. J. Appl. Phys.*, **44** (2005) 5244.
- [28] VAHEDI V., LIEBERMAN M. A., DiPESO G., ROGNLIEN T. D. and HEWETT D., *J. Appl. Phys.*, **78** (1995) 1446.
- [29] CAZZADOR M., CAVENAGO M., SERIANNI G., and VELTRI P., *AIP Conf. Proc.*, **1655** (2015) 020014.
- [30] TACCOGNA F., MINELLI P., CAVENAGO M., VELTRI P. and IPPOLITO N., *Rev. Sci. Instrum.*, **87** (2016) 02B145.
- [31] FONNESU N., CAVENAGO M., SERIANNI G. and VELTRI P., *Rev. Sci. Instrum.*, **87** (2016) 02B905.
- [32] VARIALE V., CAVENAGO M., AGOSTINETTI P., SONATO P. and ZANOTTO L., *Rev. Sci. Instrum.*, **87** (2016) 02B305.
- [33] STOCKLI M. P., HAN B. X., MURRAY S. N., PENNISI T. R., PILLER C., SANTANA M. and WELTON R. F., *AIP Conf. Proc.*, **1655** (2015) 030001.